RESEARCH ARTICLE

Special Section:

Key Points:

Correspondence to:

N. Suzuki,
nobuhiro_suzuki@brown.edu

Citation:

Understanding Stokes forces in the wave-averaged equations

Nobuhiro Suzuki[1] and Baylor Fox-Kemper[1]

[1]Department of Earth, Environmental, and Planetary Sciences, Brown University, Providence, Rhode Island, USA

Abstract The wave-averaged, or Craik-*Leibovich*, equations describe the dynamics of upper ocean flow interacting with nonbreaking, not steep, surface gravity waves. This paper formulates the wave effects in these equations in terms of three contributions to momentum: Stokes advection, Stokes Coriolis force, and Stokes shear force. Each contribution scales with a distinctive parameter. Moreover, these contributions affect the turbulence energetics differently from each other such that the classification of instabilities is possible accordingly. Stokes advection transfers energy between turbulence and Eulerian mean-flow kinetic energy, and its form also parallels the advection of tracers such as salinity, buoyancy, and potential vorticity. Stokes shear force transfers energy between turbulence and surface waves. The Stokes Coriolis force can also transfer energy between turbulence and waves, but this occurs only if the Stokes drift fluctuates. Furthermore, this formulation elucidates the unique nature of Stokes shear force and also allows direct comparison of Stokes shear force with buoyancy. As a result, the classic Langmuir instabilities of *Craik and Leibovich*, wave-balanced fronts and filaments, Stokes perturbations of symmetric and geostrophic instabilities, the wavy Ekman layer, and the wavy hydrostatic balance are framed in terms of intuitive physical balances.

1 Introduction

Away from shore, surface gravity waves affect the upper ocean currents that span the spatial scales of boundary layer turbulence [*Sullivan and McWilliams*, 2010; *D'Asaro*, 2014] to submesoscale [*Hamlington et al.*, 2014] and mesoscale eddies, fronts, and filaments [*McWilliams and Fox-Kemper*, 2013]. As these currents control transport and dispersion in the upper ocean where flotsam and light are most plentiful, correct understanding of the wave effects are critical in understanding the dispersion of pollutants and biological tracers and plankton. These waves also affect the wind-driven Ekman layer [*Polton et al.*, 2005; *McWilliams et al.*, 2012], internal waves, and symmetric instabilities [*Li et al.*, 2012; *Malecha et al.*, 2014; *Haney et al.*, 2015], and their collective effects affect the climate sensitivity of the entire earth [*Cavaleri et al.*, 2012; *Belcher et al.*, 2012; *Li et al.*, 2015]. Recent observations confirm some of the theoretical or model-based scalings directly [*Kukulka et al.*, 2009; *D'Asaro et al.*, 2014].

However, large-scale oceanography has tended to overlook surface gravity waves in favor of other dynamical balances, such as geostrophic and Ekman layer motions. This neglect is in part due to the difficulty in accurately measuring statistics of wave motions and their consequences in the turbulent upper ocean, but also in part due to the complexity of presentations of the dynamical coupling across scales from these fast, small surface waves to slower, larger motions [*Longuet-Higgins and Stewart*, 1964; *Hasselmann*, 1971; *Craik and Leibovich*, 1976; *Holm*, 1996; *Gjaja and Holm*, 1996; *Lane et al.*, 2007]. Furthermore, it is frequently assumed (in error) that wave consequences are felt only in upper few meters, where orbital velocities and Stokes drift are strong. However, the mechanisms proposed by *Craik and Leibovich* [1976] have inspired a set of asymptotic theories [*McWilliams et al.*, 2004; *Chini et al.*, 2008; *McWilliams et al.*, 2012; *McWilliams and Fox-Kemper*, 2013] and clarification of different representations of surface wave effects within these asymptotic limits [*Lane et al.*, 2007].

The influence of surface gravity waves on ocean currents occurs through several mechanisms. One of the mechanisms is the nonlinear interaction between wave orbital velocities and currents. This nonlinear interaction can be represented in several different ways, each of which allows focusing on a different aspect of the underlying physics more readily. In particular, for those currents that evolve slowly compared to the

oscillation of surface gravity waves, and when the waves are of limited steepness and do not break, the nonlinear interaction can be represented as either radiation stress or a combination of a vortex force and a modified pressure [*Lane et al.*, 2007]. The former representation has been useful in understanding phenomena like wave setup in the coastal surf zone, longshore currents, and infragravity waves [*Longuet-Higgins*, 1970], and the latter representation, known as the wave-averaged or Craik-Leibovich equations [*Craik and Leibovich*, 1976; *Leibovich*, 1980; *Holm*, 1996; *McWilliams et al.*, 2004], has been useful in understanding phenomena like Langmuir circulations and turbulence, particularly when implemented as the basis for Large Eddy Simulations [*Denbo and Skyllingstad*, 1996; *McWilliams et al.*, 1997; *Kukulka et al.*, 2009; *Harcourt and D'Asaro*, 2008; *Polton and Belcher*, 2007; *Teixeira and Belcher*, 2010; *Van Roekel et al.*, 2012]. Here the emphasis will be on the wave-averaged Boussinesq (WAB) equations. These equations are found by a multiscale asymptotic analysis, where small, fast motions are separated from larger, slower motions. If wave steepness is taken to be a small parameter, and the fast, small-scale solutions are taken to be surface gravity waves, then the WAB equations result upon filtering out the waves but retaining the leading order wave couplings with other scales [*Craik and Leibovich*, 1976; *McWilliams et al.*, 2004].

The primary emphasis in this paper will be developing the consequences and scaling of the WAB equations so as to build intuition about the kinds of Langmuir scale (10–100 m), submesoscale (100 m–10 km), and mesoscale (10–100 km) motions that result from interactions with surface gravity waves in the WAB system. Section 2 presents a new form of the WAB system as well as its energetics and vorticity dynamics, and contrasts it against extant WAB forms. Sections 3, 4, and 5 demonstrate applications of the recast WAB equations. As all of the interactions with waves in the WAB equations involve only one wave statistic—the Stokes drift—the interaction terms will be collectively referred to as Stokes forces. Other wave effects—breaking, spray, bubbles, surface roughness, etc. [*Cavaleri et al.*, 2012]—are neglected or indirectly handled in the WAB equations, and while they may be important (particularly near shore) they will not be emphasized here.

2. Recasting the WAB Equations

2.1. Extant Forms of the WAB Equations

Even when the radiation stress form is left aside, the wave-averaged Boussinesq equations have been represented in several different forms that are all mathematically equivalent (Appendix A) through vector identities [*Holm*, 1996]: namely

$$\partial_t \mathbf{u} + (\nabla \times \mathbf{u} + \mathbf{f}) \times \mathbf{u}^L = \mathbf{b} + \mathbf{D}^u - \nabla \left(p + \frac{1}{2}|\mathbf{u}^L|^2 \right), \tag{1}$$

$$\partial_t \mathbf{u} + (\mathbf{u} \cdot \nabla)\mathbf{u} + \mathbf{f} \times \mathbf{u}^L = \mathbf{b} + \mathbf{D}^u - \nabla \left(p + \frac{1}{2}|\mathbf{u}^L|^2 - \frac{1}{2}|\mathbf{u}|^2 \right) - (\nabla \times \mathbf{u}) \times \mathbf{u}^S, \tag{2}$$

$$\partial_t \mathbf{u} + (\mathbf{u}^L \cdot \nabla)\mathbf{u} + \mathbf{f} \times \mathbf{u}^L = \mathbf{b} + \mathbf{D}^u - \nabla \left(p + \frac{1}{2}|\mathbf{u}^S|^2 - \frac{1}{2}|\mathbf{u}|^2 \right) - u_j \nabla u_j^L, \tag{3}$$

$$\partial_t \mathbf{u}^L + (\mathbf{u}^L \cdot \nabla)\mathbf{u}^L + \mathbf{f} \times \mathbf{u}^L = \mathbf{b} + \mathbf{D}^u - \nabla p - \mathbf{u}^L \times (\nabla \times \mathbf{u}^S) + \partial_t \mathbf{u}^S. \tag{4}$$

Here, every flow variable is to be taken as an average over a short time (e.g., minutes) to filter out the rapid oscillation of surface gravity waves (although notation of the averaging operator is omitted); t is the time; $\nabla = (\partial_1, \partial_2, \partial_3) = (\partial_x, \partial_y, \partial_z)$ with horizontal coordinates $(x_1, x_2) = (x, y)$ and vertical coordinate $x_3 = z$; $\mathbf{f} = f\hat{\mathbf{z}}$ is the Coriolis parameter (The effects of a rotation axis not parallel to gravity can be included, as nonhydrostatic physics will be retained.); $\mathbf{b} = -g\rho/\rho_o\hat{\mathbf{z}} = b\hat{\mathbf{z}}$ is the buoyancy with the gravitational acceleration g and the constant reference density ρ_o; p is the (thermodynamic) pressure divided by ρ_o; $\mathbf{D}^u$ is the diffusion; $\mathbf{u} = (u_1, u_2, u_3) = (u, v, w)$ is the wave-filtered Eulerian velocity (i.e., Eulerian velocity of the slow currents); $\mathbf{u}^S$ is the Stokes drift; and $\mathbf{u}^L = \mathbf{u} + \mathbf{u}^S$ is the wave-filtered Lagrangian velocity. The Stokes drift and Lagrangian velocity are taken to be the average velocity of a trajectory to leading order in small wave slope [*Webb and Fox-Kemper*, 2011]. The assumption of small wave slope necessarily precludes the incorporation of breaking waves directly in these equations, except in parameterized form as suggested by *Sullivan and McWilliams* [2010]. In (3) and elsewhere, the Einstein summation convention is used; i.e., $u_j \nabla u_j^L = u_1 \nabla u_1^L + u_2 \nabla u_2^L + u_3 \nabla u_3^L$, although familiar vector notation will be used when it is unambiguous.

For these equations to be valid, there must be a separation of horizontal and temporal scales between the waves and the circulation, and the steepness of the waves must be limited [*McWilliams et al.*, 2004]. In the coastal zone, strong variations of currents and surf zones may violate these limitations, but in open water they are more easily satisfied. The conservation principles obeyed by waves are not just a conservation for Lagrangian momentum instead of Eulerian momentum [*Gjaja and Holm*, 1996; *Ardhuin et al.*, 2008], and generally the conversion between conserved wave properties (e.g., wave action) and Stokes drift are nontrivial. Even the simple example of a monochromatic wave entering a region of variable flow and interacting with weakly varying currents [*Mei*, 1989] is challenging when framed as a prediction of Stokes drift. For realistic wave spectra of multiple wave types, such analysis is generally carried out using third-generation wave models [*Komen et al.*, 1994; *Holthuijsen*, 2007]. For this reason, it is rare at present to have simulations where the waves are simulated within the same model as the currents, rather than as a separate wave model coupled to a circulation model. By assuming that shear zones are wide when compared to wavelength and wave energy is large when compared to the energy extracted during the interactions considered, the wave action and thus Stokes drift can be considered unaffected by variations in currents to leading order [*McWilliams et al.*, 2004].

Equations (1), (2), (3), and (4) are identical through vector identities but differ significantly in interpretation. In (1), the forces are organized in a way that is often used in the regular (i.e., without rapidly oscillating surface waves) Eulerian dynamics. Then, the wave-current nonlinear interaction is regarded as a modification of the regular vortex force, $(\nabla \times \mathbf{u}) \times \mathbf{u}$, to a wave-influenced one, $(\nabla \times \mathbf{u}) \times \mathbf{u}^L$, accompanied by a modification of the pressure. This form also allows a straightforward combination of the Coriolis force and the vortex force as $(\nabla \times \mathbf{u} + \mathbf{f}) \times \mathbf{u}^L$. Equation (2) shows the dynamics of the slow currents, following the filtered Eulerian velocity $(\partial_t + \mathbf{u} \cdot \nabla)\mathbf{u}$. For these reasons, (1) and (2) are popular [e.g., *McWilliams et al.*, 1997; *McWilliams and Fox-Kemper*, 2013]. The form of (3) is closest to the exact wave-current interaction theory known as the Generalized Lagrangian Mean theory [*Andrews and McIntyre*, 1978; *Ardhuin et al.*, 2008] and is useful in showing that the WAB equations are an asymptotic approximation to the exact theory [*Leibovich*, 1980; *Holm*, 1996]. Finally, (4) reveals the similarity in wave-current interaction to the Lorentz force in plasma physics [*Holm*, 1996]. Other closely related forms are discussed in *Garrett* [1976]; *Smith* [2006]; and *Ardhuin et al.* [2008].

Although each form of the foregoing WAB equations has its own strength, the groupings of forces used in these forms do not immediately reveal the mechanisms of the wave-induced instabilities known as the CL instabilities [*Leibovich*, 1983], nor the wave-balanced solutions that obey a Lagrangian thermal wind relation to leading order [*McWilliams and Fox-Kemper*, 2013], nor the wavy Ekman layer [*McWilliams et al.*, 2012]. For example, the CL instabilities are distinguished from boundary-layer shear-flow turbulence by their extraction of wave energy, instead of kinetic energy in the Eulerian mean shear; thus, diagnosis of instability mechanisms requires distinction between the force that transfers wave energy and the force that transfers Eulerian mean kinetic energy. The vortex force in (1) or (2) mixes these forces together. Although the vorticity budget is easily found from (1) or (2), the energy budget is not. Likewise, in (3), the term $-u_j \nabla u_j^L$ drives the CL instabilities. However, this term also contains a conservative force $-\nabla|\mathbf{u}|^2/2$ $(=-u_j \nabla u_j)$, which does not transfer wave energy. In addition, the grouping of $|\mathbf{u}^S|^2/2$ with the pressure introduces a wave influence in the pressure energy transport and prevents clear separation of the wave effects from other effects in the energetics. Similarly, the advection term in (4) does not distinguish the energy transfers from wave energy and Eulerian mean kinetic energy. Therefore, to distinguish the consequences of wave energy transfer from those of other factors and to understand how wave energy drives some oceanic circulations, it is desirable to reorganize the foregoing forms of the WAB equations in a new manner. To this end, an alternative form of the WAB equations is presented in the next section.

2.2. The Alternative Form

The alternative form separates the wave interaction force due to the Coriolis effect from that irrelevant to the Coriolis effect like equations (2–4). However, unlike the other forms, the alternative form divides the latter force into the part that pertains to wave energy transfer and the part that does not. The alternative form is mathematically equivalent to (1)-(4), yet it more readily reveals the essence of the dynamics, energetics, and scaling of the CL instabilities (section 3). Moreover, the alternative form simplifies analysis of wave effects on the buoyancy-related dynamics such as hydrostatic balance, fronts, and filaments studied by *McWilliams and Fox-Kemper* [2013] (N. Suzuki et al., Surface waves affect frontogenesis, J. Geophys. Res. Oceans, submitted, 2016) (section 4). Finally, it highlights the conditional (dependent on flow fluctuation)

and directional (dependent on alignment of flow fluctuation and Stokes shear) nature of wave effects, providing insight into wave effects on Reynolds stresses and instabilities under varying shear (section 5).

The WAB momentum equations (1)–(4) are mathematically equivalent to:

$$\partial_t \mathbf{u} + \underbrace{(\mathbf{u}^L \cdot \nabla)\mathbf{u}}_{\text{Lagrangian advection}} = \underbrace{-\mathbf{f} \times \mathbf{u}^L}_{\text{Lagrangian Coriolis}} + \mathbf{b} + \mathbf{D}^u - \nabla p \underbrace{- u_j^L \nabla u_j^S}_{\text{Stokes shear}}. \tag{5}$$

This form may be derived from (3) using vector identities $\nabla|\mathbf{u}|^2/2 = u_j \nabla u_j$ and $\nabla|\mathbf{u}^S|^2/2 = u_j^S \nabla u_j^S$, or from (4) using $\mathbf{u}^L \times (\nabla \times \mathbf{u}^S) = u_j^L \nabla u_j^S - (\mathbf{u}^L \cdot \nabla)\mathbf{u}^S$ (Appendix A). The derivations from (1) and (2) are shown in Appendix A. The wave effects in (5) are framed in terms of three forces which have distinct roles in the dynamics and energetics of wave-influenced flows: namely, $(\mathbf{u}^L \cdot \nabla)\mathbf{u}$ (hereafter, Lagrangian advection), $-\mathbf{f} \times \mathbf{u}^L$ (hereafter, Lagrangian Coriolis force), and $-u_j^L \nabla u_j^S$ (hereafter, Stokes shear force). Lagrangian Coriolis force represents the wave-influenced Coriolis effect. The wave forcing that is independent from the Coriolis effect is divided in two parts according to their roles in energetics. Namely, Stokes shear force is the part that transfers wave energy to Eulerian velocities, and Stokes advection $(\mathbf{u}^S \cdot \nabla)\mathbf{u}$ is the part that does not transfer wave energy (section 2.4).

Stokes advection is combined with Eulerian advection $(\mathbf{u} \cdot \nabla)\mathbf{u}$ and handled as Lagrangian advection as in (3). This is partly because Stokes advection and Eulerian advection can produce same instabilities which feed on kinetic energy of the Eulerian mean shear (section 2.4), and partly because Lagrangian advection of momentum mirrors the wave-averaged advection of buoyancy (b) and other quantities such as salinity (s), absolute vorticity (ω^a), and potential vorticity (q):

$$\partial_t b + (\mathbf{u}^L \cdot \nabla)b = D^b, \tag{6}$$

$$\partial_t s + (\mathbf{u}^L \cdot \nabla)s = D^s, \tag{7}$$

$$\partial_t \omega^a + (\mathbf{u}^L \cdot \nabla)\omega^a = (\omega^a \cdot \nabla)\mathbf{u}^L + \nabla \times \mathbf{b} + \nabla \times \mathbf{D}^u, \quad \omega^a \equiv \mathbf{f} + \nabla \times \mathbf{u}, \tag{8}$$

$$\partial_t q + (\mathbf{u}^L \cdot \nabla)q = D^q = \nabla \cdot (\mathbf{D}^u \times \nabla b + \omega^a D^b), \quad q \equiv \omega^a \cdot \nabla b, \tag{9}$$

where D^b and D^s are diffusion of buoyancy and salinity, respectively. A similar expression to equations (6), (7), and (9) is expected for any materially conserved quantity, because the Lagrangian velocity measures the displacement of water parcels in time [e.g., *Holm*, 1996; *Eames and McIntyre*, 1999; *Webb and Fox-Kemper*, 2011]. Note that vorticity and potential vorticity are formed from the curl of the Eulerian velocity, not the Lagrangian velocity.

2.3. Scaling the Alternative Form

A dimensionless form of the recast WAB equations is illustrative. Following scalings from *McWilliams* [1985]; *McWilliams and Fox-Kemper* [2013]; and *Haney et al.* [2015], but separately scaling the horizontal and vertical momentum equations,

$$\partial_t b + (\mathbf{u}^L \cdot \nabla)b = \frac{1}{\text{Pe}} D^b, \tag{10}$$

$$\text{Ro}\left[\partial_t u_h + (\mathbf{u}^L \cdot \nabla)u_h + \text{Eu}\partial_h p + \frac{V^S}{V^L}\frac{\ell}{\ell^S} u_j^L \partial_h u_j^S\right] = -\varepsilon_{h3j} u_j^L + \frac{\text{Ro}}{\text{Re}} D_h^u, \tag{11}$$

$$\frac{H^2}{\ell^2}\left[\partial_t w + (\mathbf{u}^L \cdot \nabla)w\right] + \text{Eu}[\partial_z p - b] + \frac{V^S}{V^L}\frac{H}{H^S} u_j^L \partial_z u_j^S = \frac{H^2}{\ell^2 \text{Re}} D_3^u, \tag{12}$$

$$\partial_h u_h + \frac{\partial w}{\partial z} = 0, \tag{13}$$

where $h = 1, 2$; $j = 1, 2, 3$; ε_{hij} is the Levi-Civita symbol; $\mathbf{D}^u = (D_1^u, D_2^u, D_3^u)$; Pe is the Peclet number; Re is the Reynolds number; $\text{Ro} = V^L/f\ell$ is the Rossby number; Eu is the Euler number and can be taken to be $\max(1, \text{Ro}^{-1})$ in Langmuir, submesoscale, and mesoscale motions; V^S is the velocity scale of the Stokes drift; V^L is the scale of Lagrangian velocity as well as Eulerian velocity; H and H^S are the depth scales of the Eulerian flow and Stokes drift; ℓ and ℓ^S are the horizontal scales of the Eulerian flow and Stokes drift; and ℓ/V^L is

the (advective) time scale. For simplicity in scaling, the planetary rotation axis is taken in this section only to be in the vertical direction; other sections preserve a vector Coriolis parameter with arbitrary orientation.

While the emphasis here is on the field equations, some discussion of typical boundary conditions is appropriate. Surface wind stresses are typically taken to match with viscous Eulerian shear stresses [*Craik and Leibovich*, 1976; *McWilliams et al.*, 1997], and surface thermal forcing is represented in the usual way. However, the heat and momentum transfer from winds via pressure form drag, viscosity, and breaking waves is much more complicated in reality [*Sullivan et al.*, 2007; *Cavaleri et al.*, 2012]. Bottom boundary conditions are ordinarily standard, as Stokes effects are typically small at the bottom of the domain, although not always [*Tejada-Martinez and Grosch*, 2007]. Care must be taken when sidewalls or shallow water are considered, because wave steepening and breaking will invalidate the asymptotic assumptions of the WAB system, so typically horizontal periodic boundary conditions are used. Atmospheric surface pressure conditions are imposed on the wave-averaged state as normal, following examination of wave averages [*Craik and Leibovich*, 1976]. Sometimes a rigid lid approximation is used, or suitable kinematic boundary conditions which to leading order amount to vertical velocity balancing the sum of convergences in the mass transport of waves due to varying Stokes drift and dynamic or bottom-slope induced convergences of Eulerian currents [*Lane et al.*, 2007].

In the open ocean, Stokes drift is persistent, as surface wave packets often share the length scales of the atmospheric synoptic variability and wave-current interactions are relatively weak. Estimates of ℓ^S from global wave models yield $O(1000\ km)$ values and the time scale of Stokes drift persistence is greater than $O(10\ d)$ [*Haney et al.*, 2015]. In contrast, H^S is $O(3\ m)$ and is much smaller than H which may be taken as the boundary layer depth for Langmuir turbulence: $O(30\ m)$, the mixed layer depth for submesoscales: $O(70\ m)$, and the pycnocline depth for mesoscales: $O(500\ m)$. Thus, the horizontal Stokes shear force in (11) is expected to be weak over the range of scales from Langmuir to mesoscale.

The vertical Stokes shear force in (12), however, is typically significant. At the Langmuir scale, the Stokes shear force in (12) is $O(V^S H/(V^L H^S)) \gg 1$ when compared to the buoyancy within the upper part of the mixed layer where the Stokes drift exists (assuming $V^S \approx V^L$). Thus, the effect of the vertical Stokes shear force is expected to be nonhydrostatic within the upper ocean where Stokes shear is large. If an integrated budget over the mixed layer is considered, the H/H^S factor drops out and the depth-integrated Stokes shear force is of similar order to the depth-integrated force due to buoyancy [*Suzuki et al.*, 2016] or nonhydrostatic pressure gradient, and their relationship may be scaled by the equivalent here of the inverse square of the turbulent Langmuir number: V^S/V^L [*McWilliams et al.*, 1997; *Belcher et al.*, 2012].

At the submesoscale and mesoscale, the Stokes shear force scales as $\epsilon = \mathrm{Ro}\,V^S H/(V^L H^S)$ versus the buoyancy force. While this term may be small if Ro is small, it is generally larger than Ro, as argued above and shown from observations in *McWilliams and Fox-Kemper* [2013]. Thus, we may expect that the Stokes shear force in (12) enters the mesoscale and submesoscale dynamics earlier than finite Rossby effects enter in (11). In vertically integrated budgets, again the H/H^S factor drops out and one expects an $O(\mathrm{Ro})$ nonhydrostatic Stokes shear force. This ratio may be rearranged to highlight that it is a wave statistic times the aspect ratio or frontal isopycnal slope: $\epsilon = V^S/(fH^S) \cdot (H/\ell)$. (These scaling assertions are evaluated quantitatively for a series of modeled fronts in *Suzuki et al.* [2016].)

In Large Eddy Simulations with $O(1\ m)$ vertical and horizontal resolution, (10)–(13) may be solved directly. However, it is interesting to contemplate how the Stokes forces may be included in large-scale and global models where $H^2/\ell^2 \ll 1$. Many models are now capable of enhanced vertical mixing driven by waves [*Huang et al.*, 2011; *Fan and Griffies*, 2014; *Li et al.*, 2015]. However, few have attempted to directly add the Stokes forces into the resolved momentum equations. *Breivik et al.* [2015] is an excellent recent example of implementation and assessment of the Stokes Coriolis force versus other wave effects, but Stokes advection and Stokes shear force are not attempted. Indeed, it is unwise to add Stokes advection into a model where the Stokes Coriolis force is missing, because of the feedback and anti-Stokes effects that alter the overall effects of Lagrangian advection [*Monismith et al.*, 2007; *Lentz and Fewings*, 2012; *McWilliams and Fox-Kemper*, 2013; *Haney et al.*, 2015]. Comparison of Stokes drift to Eulerian currents is useful for scaling [*McWilliams and Restrepo*, 1999], but these currents are not simply additive. Feedback from the Stokes shear force to advection may be important as well [*McWilliams and Fox-Kemper*, 2013]. Some have tried to formulate the large-scale wave-averaged equations without retaining nonhydrostatic effects [e.g., *Mellor*, 2003], but the

preceding arguments about the scaling of the Stokes shear force in (12) suggest that nonhydrostatic Stokes shear force effects are the most important ones. Building intuition about these forces is the focus of this paper.

The scaling in (12) suggests a quasi-hydrostatic, or "wavy hydrostatic," alternative for large-scale modeling when $H \ll \ell$. If the $O(H^2/\ell^2)$ terms are neglected but the $O(\epsilon)$ Stokes shear force term is retained, then the Stokes shear force *alone* violates the hydrostatic balance.

$$\partial_z p \approx b - \frac{V^S}{\text{Eu}V^L}\frac{H}{H^S}u_j^L \partial_z u_j^S. \tag{14}$$

This version of the equation remains diagnostic, rather than prognostic, just as the hydrostatic balance is, so it may be implemented in general circulation models just by adding the Stokes shear force wherever the buoyancy appears.

2.4. Energetics of Stokes Forces

The distinct roles of Stokes forces can be highlighted by considering, especially, the energetics of filtered Eulerian flows. The mean-flow kinetic energy (MKE), turbulence kinetic energy (TKE), and wave energy (WE) per unit mass are defined as $E_{\text{MKE}} \equiv |\langle \mathbf{u} \rangle|^2/2$ and $E_{\text{TKE}} \equiv |\mathbf{u}'|^2/2$, $E_{\text{WE}} \equiv gH_{m0}^2/(16H)$ respectively, where the angle brackets denote an averaging, $\mathbf{u}' \equiv \mathbf{u} - \langle \mathbf{u} \rangle$ is the turbulent velocity, H_{m0} is the significant wave height ($\sqrt{2}$ times the root mean squared wave height *Bouws* [1998]), and H is the budget depth. For simplicity, let us consider an averaging that commutes with differential operators $\partial_t, \partial_x, \partial_y,$ and ∂_z and also satisfies $\langle\langle\phi\rangle\rangle = \langle\phi\rangle$ and $\langle\psi\langle\phi\rangle\rangle = \langle\psi\rangle\langle\phi\rangle$ for any quantities ϕ and ψ. (An example of such averaging is the horizontal averaging over a horizontally periodic domain.) Now let us consider the rate of change of MKE and mean TKE due to Stokes forces. Namely, $\partial_t E_{\text{MKE}}$ and $\partial_t\langle E_{\text{TKE}}\rangle$ due to Lagrangian advection are:

$$\partial_t E_{\text{MKE}} = \langle\langle u_i \rangle(-u_j^L \partial_j u_i)\rangle = \underbrace{\langle u_i' u_j^{l'} \rangle \partial_j \langle u_i \rangle}_{-\text{MKE-TKE conversion}} \underbrace{-\langle u_j^L \rangle \partial_j E_{\text{MKE}}}_{\text{MKE advection}} \underbrace{-\langle u_j^{l'} \partial_j (\langle u_i \rangle u_i') \rangle}_{\text{MKE transport by stress}} \tag{15}$$
$$\rightarrow \langle u_h' w' \rangle \partial_z \langle u_h \rangle \quad + 0 \quad -\partial_z(\langle u_h \rangle \langle u_h' w' \rangle),$$

$$\partial_t \langle E_{\text{TKE}} \rangle = \langle u_i'(-u_j^L \partial_j u_i) \rangle = \underbrace{-\langle u_i' u_j^{l'} \rangle \partial_j \langle u_i \rangle}_{\text{MKE-TKE conversion}} \underbrace{-\langle u_j^L \partial_j E_{\text{TKE}} \rangle}_{\text{TKE advection}} \tag{16}$$
$$\rightarrow -\langle u_h' w' \rangle \partial_z \langle u_h \rangle - \partial_z \langle w' E_{\text{TKE}} \rangle.$$

Likewise, $\partial_t E_{\text{MKE}}$ and $\partial_t\langle E_{\text{TKE}}\rangle$ due to Stokes shear force are:

$$\partial_t E_{\text{MKE}} = \langle\langle u_i \rangle(-u_j^L \partial_i u_j^S)\rangle = \underbrace{-\langle u_i \rangle(\langle u_j^L \rangle \partial_i \langle u_j^S \rangle + \langle u_j^{l'} \partial_i u_j^{S'} \rangle)}_{\text{MKE-WE conversion}} \tag{17}$$
$$\rightarrow 0,$$

$$\partial_t \langle E_{\text{TKE}} \rangle = \langle u_i'(-u_j^L \partial_i u_j^S) \rangle = \underbrace{-\langle u_i' u_j^L \partial_i u_j^S \rangle}_{\text{TKE-WE conversion}} \tag{18}$$
$$\rightarrow -\langle u_h' w' \rangle \partial_z \langle u_h^S \rangle.$$

Finally, $\partial_t E_{\text{MKE}}$ and $\partial_t\langle E_{\text{TKE}}\rangle$ due to Stokes Coriolis force are:

$$\partial_t E_{\text{MKE}} = \langle\langle \mathbf{u} \rangle \cdot (-\mathbf{f} \times \mathbf{u}^S)\rangle = \underbrace{-\langle \mathbf{u} \rangle \cdot (\mathbf{f} \times \langle \mathbf{u}^S \rangle)}_{\text{Stokes Coriolis work I}}, \tag{19}$$

$$\partial_t \langle E_{\text{TKE}} \rangle = \langle \mathbf{u}' \cdot (-\mathbf{f} \times \mathbf{u}^S) \rangle = \underbrace{-\langle \mathbf{u}' \cdot (\mathbf{f} \times \mathbf{u}^{S'}) \rangle}_{\text{Stokes Coriolis work II}} \tag{20}$$
$$\rightarrow 0.$$

In these equations, $i, j = 1, 2, 3$ and $h = 1, 2$. Note that, in deriving the first lines of equations (15–20) from equation (5), no additional assumptions on the flow conditions are made. If we assume additional conditions that are typical for open ocean conditions—namely, $\langle w \rangle = 0$, $\langle w^S \rangle = 0$, $\nabla \cdot \mathbf{u} = 0$, $\nabla \cdot \mathbf{u}^S = 0$, $\mathbf{u}^{S'} = (0, 0, 0)$—

and use horizontal averaging over a horizontally periodic domain, then the terms in equations (15)–(20) simplify to the forms shown after the arrows.

The first terms of the right hand sides of (15) and (16) are identical with opposite signs, showing that Lagrangian advection transfers energy between MKE and mean TKE. This energy transfer—known as the TKE shear production—is the energy source of boundary-layer shear-flow turbulence. That is, boundary-layer shear-flow turbulence does not feed on WE, but it feeds on MKE and eventually dissipates the mean flow. Notice that the TKE shear production as well as all the other terms in (15) and (16) are irrelevant to WE. These terms exist with or without waves, as can be seen by setting $\mathbf{u}^S=0$ (hence $\mathbf{u}^L=\mathbf{u}$) in (15) and (16). Therefore, Eulerian advection $(\mathbf{u}\cdot\nabla)\mathbf{u}$ and Stokes advection $(\mathbf{u}^S\cdot\nabla)\mathbf{u}$ play an identical role in the energetics and linear momentum dynamics.

In contrast, the terms in (17) to (20) are unique to the wave effect; i.e., they all vanish if $\mathbf{u}^S=0$. Most importantly, and unlike the MKE-TKE conversion term, no term in (17) to (20) appears twice in (15)–(20). This shows that Stokes shear force and Lagrangian Coriolis force do not transfer energy between MKE and mean TKE. They, instead, transfer energy between WE and TKE or WE and MKE. Especially, when $u^{S\prime}=0$, Stokes Coriolis force energizes only MKE and Stokes shear force energizes only TKE. In summary, the wave effect in the WAB equations is composed of three forces whose roles in the instability mechanisms are distinctively different:

1. Lagrangian advection is the agent that converts energy between MKE and TKE. Hence, it is responsible for a group of instabilities due to MKE-TKE conversion. For a horizontally uniform mean flow (i.e., $\partial_x\langle u_i\rangle=\partial_y\langle u_i\rangle=0$), the contribution from Stokes advection vanishes unless $w^{S\prime}\neq 0$.
2. Stokes shear force transfers energy between TKE and WE. It does not transfer MKE. Hence, it is responsible for a group of instabilities due to WE-TKE conversion. This instability mechanism exists only when there is a shear in the Stokes drift.
3. Stokes Coriolis force may introduce another type of energy transfer between TKE and WE if $f\neq 0$ and $u^{S\prime}\neq 0$. Otherwise, Stokes Coriolis force transfers energy only between WE and MKE.

Because we assume steady Stokes drift, it is assumed that $E_{WE}\gg E_{MKE}, E_{TKE}$ (roughly a significant wave height over 1 m for 0.1 m s^{-1} turbulent or mean velocity in a 100 m mixed layer), or if the waves are simultaneously recharging energy removed by currents from the wind, e.g., in fully developed wind waves, then even weaker waves may be consistent with constant Stokes drift under the extraction of energy by currents.

In addition to separating the wave influence into the energetically distinct forces, the recast equation (5) offers yet another benefit. Namely, the effects of the horizontal and vertical gradients of the Stokes drift are cleanly separated. Notice that Stokes shear force is $-u_j^L\nabla u_j^S=(-u_j^L\partial_x u_j^S, -u_j^L\partial_y u_j^S, -u_j^L\partial_z u_j^S)=(-\mathbf{u}^L\cdot(\partial_x\mathbf{u}^S), -\mathbf{u}^L\cdot(\partial_y\mathbf{u}^S), -\mathbf{u}^L\cdot(\partial_z\mathbf{u}^S))$. Thus, its horizontal components are due to the horizontal gradients of the Stokes drift, and its vertical component is due to the vertical gradient of the Stokes drift. This separation is useful because the horizontal and vertical gradients of the Stokes drift often have a counteracting effect on turbulence production; i.e., when one energizes a turbulence structure, the other one suppresses it (see section 3 for such an example). In fact, the horizontal and vertical gradients of the Stokes drift lead to different types of turbulence (section 3). Moreover, in many applications, there is a scale separation between the horizontal and vertical gradients of the Stokes drift: i.e., for typical ocean conditions, $|\partial_z\mathbf{u}^S|\gg|\partial_h\mathbf{u}^S|$ where $h=1, 2$, as already shown in section 2.3. Then, the framework of Stokes shear force allows us to readily (1) separate the leading-order effect due to the dominant gradient of the Stokes drift from the higher-order effect and (2) classify instabilities based on the Stokes drift gradients. The modes by which Stokes forces make energy available for turbulence are listed in Table 1.

Table 1. Modes by Which Stokes Forces Make Energy Available for Turbulence[a]

Energy Source	Necessary Condition	Responsible Force
MKE	$\mathbf{u}^{S\prime}\neq 0$	Stokes advection $(\mathbf{u}^S\cdot\nabla)\mathbf{u}$
WE	$\mathbf{u}^{S\prime}\neq 0$ and $f\neq 0$	Stokes Coriolis force $-\mathbf{f}\times\mathbf{u}^S$
WE	$\partial_h\mathbf{u}^S\neq 0$	Horizontal Stokes shear force $-u_j^L\partial_h u_j^S$ with $h=1, 2$
WE	$\partial_z\mathbf{u}^S\neq 0$	Vertical Stokes shear force $-u_j^L\partial_z u_j^S$

[a]Note that each group listed here may form a hybrid with another group or other forces such as buoyancy, Eulerian advection, and diffusion.

2.5. Vorticity From Stokes Forces

Let us briefly consider the vorticity dynamics framed in terms of Stokes advection, Stokes Coriolis force, and Stokes shear force. *Holm* [1996] presents the WAB vorticity equation in the form of (8). This form expresses the vorticity dynamics in terms of familiar notions of vortex advection, stretching, and tilting, but mixes the effects of Stokes advection and Stokes shear force. If the vorticity equation (8) is formed without combining Stokes forces, then they individually contribute as:

$$\nabla \times (\mathbf{f} \times \mathbf{u}^L) = (\mathbf{u} \cdot \nabla)\mathbf{f} - (\mathbf{f} \cdot \nabla)\mathbf{u} + \mathbf{f}(\nabla \cdot \mathbf{u})$$
$$+ (\mathbf{u}^S \cdot \nabla)\mathbf{f} - (\mathbf{f} \cdot \nabla)\mathbf{u}^S + \mathbf{f}(\nabla \cdot \mathbf{u}^S), \tag{21}$$

$$\nabla \times [(\mathbf{u}^L \cdot \nabla)\mathbf{u}] = (\mathbf{u} \cdot \nabla)\omega - (\omega \cdot \nabla)\mathbf{u} + \omega(\nabla \cdot \mathbf{u})$$
$$+ (\mathbf{u}^S \cdot \nabla)\omega - (\omega \cdot \nabla)\mathbf{u}^S + \omega(\nabla \cdot \mathbf{u}^S) + (\nabla u_j^S) \times (\nabla u_j), \tag{22}$$

$$\nabla \times (-u_j^L \nabla u_j^S) = (\nabla u_j^S) \times (\nabla u_j). \tag{23}$$

where $\boldsymbol{\omega} = \nabla \times \mathbf{u}$. Thus, the curl of Lagrangian Coriolis and advection contain the familiar advection, tilting, and stretching of planetary and relative vorticity, respectively, by the Eulerian velocity and the Stokes velocity. In addition, the curl of Lagrangian (or rather Stokes) advection has an unfamiliar term which is singled out by the curl of the Stokes shear force.

To highlight this point, consider a simple 2-D Langmuir circulation ($\partial_x \mathbf{u} = 0$) in which the Stokes drift $\mathbf{u}^S = (u^S, 0, 0)$ is horizontally uniform and aligned with the axes of the Langmuir circulation. In this case, the Stokes advection is exactly zero, thus, so is its curl. Yet, exactly this situation is often rationalized by considering the effect of tilting and stretching that results from Stokes advection [e.g., *Thorpe*, 2004]! The paradox is resolved by noting that, in this case, the unfamiliar term exactly cancels the tilting and stretching by the Stokes velocity. On the other hand, the curl of the Stokes shear force is nonzero if $\partial_z u^S \neq 0$ and $\partial_y u \neq 0$ as expected for a Langmuir circulation. Therefore, it is the Stokes shear force—not the curl of the Stokes advection—that injects vorticity into this canonical Langmuir circulation and validates the tilting and stretching interpretation by canceling the unfamiliar term.

Relatedly, the careful reader may have wondered why the Stokes shear force does not appear explicitly as a source of potential vorticity in equation (9). The Stokes shear force on its own does produce potential vorticity, but so too does Stokes advection–by the unfamiliar term (by design tilting and stretching never produce potential vorticity). Thus, the combination of Stokes shear force and Stokes advection is not a source of potential vorticity, but Stokes advection would be a source in the absence of the Stokes shear force.

Since the vortex force forms of the WAB equations, (1) and (2), are mathematically identical to the Stokes shear form, the vorticity equations must likewise be identical. Thus, any terms that appear inside the gradient in (1) and (2) do not contribute to the vorticity budget, and any net source of vorticity or potential vorticity must have an analog in the other equation form. In some situations, interpretation of vorticity budgets may be simpler using the curl of the Stokes vortex force. However, because all of the scalar advection equations-salinity, buoyancy, potential vorticity–share the same form in the Lagrangian advection formulation, it is helpful to preserve Lagrangian advection throughout the equations which is not true of the Stokes vortex formulations.

3. Revisiting the Craik-Leibovich (CL) Instabilities

This section revisits the canonical CL instabilities [*Leibovich*, 1983] and associated Langmuir circulation in the recast form of the WAB equations. The goals are to better understand these processes and to exemplify the recast equations, but solutions of these equations are found elsewhere [e.g., *Craik and Leibovich*, 1976; *Leibovich*, 1983].

First, let us consider the wave influence on the energetics: i.e., equations (15)–(20). For the canonical cases of the CL instabilities, the flow is configured such that w^S, $\mathbf{f}$, $\langle w \rangle$, $\nabla \cdot \mathbf{u}$, and $\nabla \cdot \mathbf{u}^S$ are all zero, where the angle bracket is the horizontal average. In this configuration, all the terms on the right hand sides of (15) and (16) reduce to the regular Eulerian ones and show no wave influence. Also, all the terms in (19) and (20) become zero. Thus, the only mean TKE equation that shows a wave influence is (18). This means that Stokes
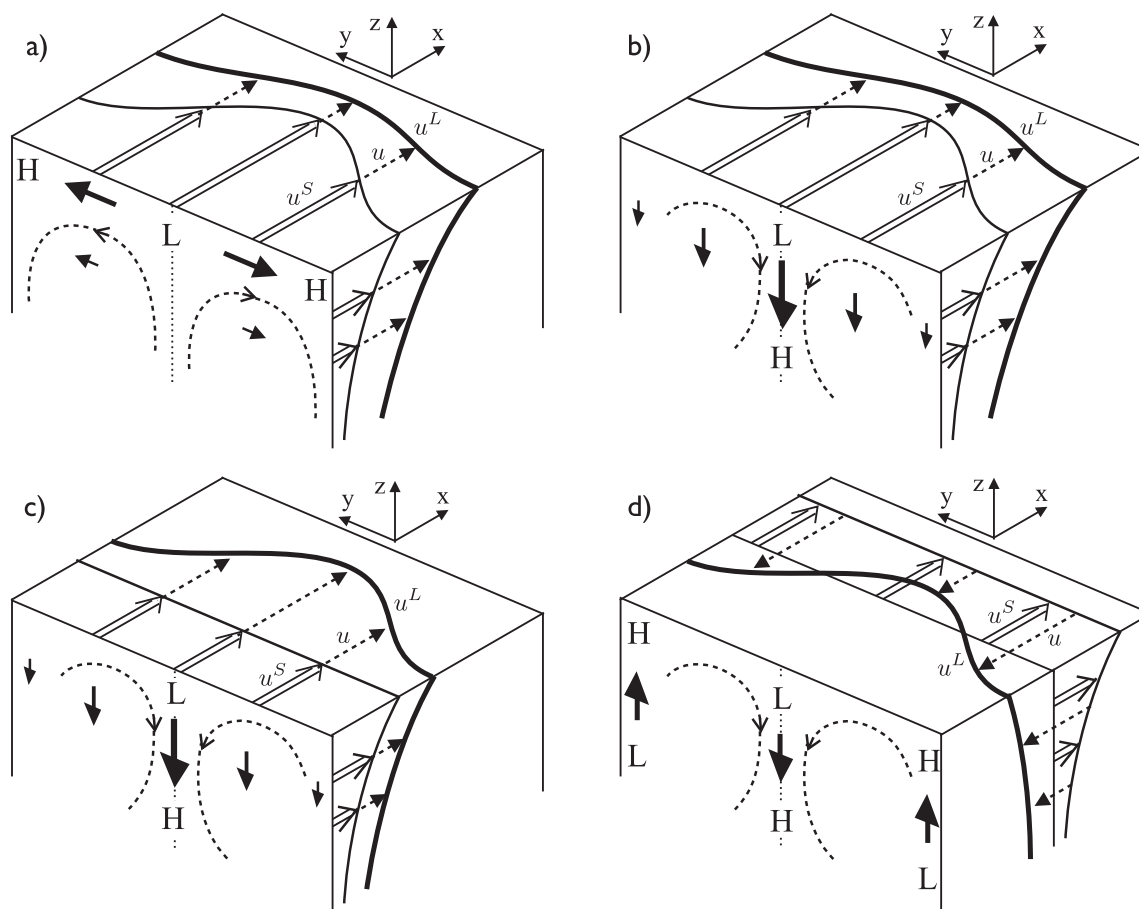
Figure 1. Sketch illustrating the CL instability mechanisms for example flows. In the examples, the Stokes drift (double-line arrow) is $\mathbf{u}^S(y,z)=(u^S,0,0)$. Thus, a field of Stokes shear force (solid arrow) is generated on the y-z plane as $(0, -u^L\partial_y u^S, -u^L\partial_z u^S)$. Then the Stokes shear force drives a circulation (dashed line) and pressure perturbation (H for high and L for low) on the y-z plane. (a) The horizontal component of the Stokes shear force for the given $\mathbf{u}^S$ and u^L. (b) The vertical component of the Stokes shear force for the same $\mathbf{u}^S$ and u^L as in Figure 1a. Notice that the induced circulation has the opposite sense of rotation from that of Figure 1a. (c) A case having a horizontally uniform Stokes drift. For a horizontally uniform Stokes drift, the Stokes shear force has the vertical component only. (d) A case having a horizontally uniform Stokes drift, but with a negative horizontally averaged u.

shear force—not Stokes advection nor Stokes Coriolis—is responsible for energizing the canonical CL instabilities.

The canonical configuration also assumes that the Stokes drift has a form $\mathbf{u}^S=(u^S(y,z),0,0)$. Thus, the Stokes shear force is simply $(0, -u^L\partial_y u^S, -u^L\partial_z u^S)$. Because the Stokes drift decays with depth, forcing is typically strongest near the surface (although a subsurface maximum is possible with multidirectional waves: *Webb and Fox-Kemper*, [2015]).

Consider the example shown in Figure 1a, illustrating the Stokes shear force due to horizontal variation in Stokes drift: namely, $(0, -u^L\partial_y u^S, 0)$. On the right side of Figure 1a, both u^L and $\partial_y u^S$ are positive, leading to a vertically decaying Stokes shear force in the negative y-direction. On the left side, the Stokes shear force is positive in the y-direction as $\partial_y u^S < 0$. Hence, the Stokes shear force pushes the water away from the top-middle part of the y-z plane. At the same time, to satisfy the incompressibility, the divergence and convergence of the Stokes shear force induce a pressure perturbation as shown in the figure to drive the upwelling in the middle and downwelling on the sides. As the Stokes shear force and the induced circulation are in the same direction, the work done by the Stokes shear force to the induced circulation is positive, leading to a further enhancement of the circulation. This mechanism is the basis of the CL1 instability. Pressure work merely redistributes this energy input by the Stokes shear force over the entire circulation. As indicated by the scale analysis in section 2.3, the horizontal component of the Stokes shear force in open ocean is small, and CL1 instability is thus unimportant.

Figure 1b illustrates the Stokes shear force due to the vertical gradient of the Stokes drift for the same u^S and u^L. This time, the Stokes shear force $(0, 0, -u^L \partial_z u^S)$ is vertical and negative everywhere but is strongest at the top-center part of the y-z plane. Hence, the Stokes shear force pushes down the water there, and its divergence and convergence induce pressures drawing water horizontally into the top-center and push away water from the lower-center. Again, the Stokes shear force energizes the induced circulation toward instability, this time associated with the CL2 mechanism of *Leibovich* [1983].

The sense of circulation is opposite between Figures 1a and 1b. Hence, the horizontal and vertical gradients of the Stokes drift compete with each other; the unstable circulation is that of Figure 1a when $|\partial_y u^S| \gg |\partial_z u^S|$ and Figure 1b when $|\partial_y u^S| \ll |\partial_z u^S|$. The scale analysis in section 2.3 indicates that the class of instability with $|\partial_y u^S| \ll |\partial_z u^S|$ is dominant under typical wind forcing (consistently with the findings of *Leibovich* [1983]).

The recast formulation allows easy consideration of two more examples (Figures 1c and 1d) with horizontally uniform Stokes drift (hence, the horizontal Stokes shear force is zero). Figure 1c has both **u** and **u**^{S} oriented in the down-wind, wave-aligned direction and is the configuration of the canonical CL2 instability [*Leibovich*, 1983]. Its instability mechanism is identical to Figure 1b. Figure 1d has **u** opposing **u**^{S}, as in anti-Stokes flow or other oppositely directed wave and current [e.g., *Monismith et al.*, 2007; *Lentz and Fewings*, 2012; *McWilliams and Fox-Kemper*, 2013]. Even in this case, the instability mechanism is essentially the same as that in Figures 1b and 1c. The average Stokes shear force is simply cancelled by the wavy hydrostatic pressure (14) to satisfy incompressibility (13) and is dynamically unimportant–only the deviation from this average drives circulation.

Eulerian processes are still at work in addition to the wave-induced process described above and may act against or constructively with the Stokes shear force. Coupling with other forces is discussed more in section 5.

4. Revisiting Wave-Influenced Surface Filaments and Fronts

This section revisits the solutions to the WAB equations from *McWilliams and Fox-Kemper* [2013], which show that the steady state of a surface front or filament under wave influence is perturbed away from thermal wind balance. Again, the goals are to better understand these processes and to exemplify the recast equations; solutions of these equations are found elsewhere [e.g., *McWilliams and Fox-Kemper*, 2013; *Haney et al.*, 2015; *Suzuki et al.*, 2016]. The *McWilliams and Fox-Kemper* [2013] solution involves an elliptic boundary-value problem for the density perturbation, with relatively intensive mathematical manipulation of the momentum equation in the form (1), as well as the buoyancy (6), potential vorticity (9), and incompressibility (13) equations. This section sketches the essential wave influence in the framework of the recast equation (5) to provide an intuitive physical approach to this problem. For brevity, only a filament will be considered since the mechanisms of the wave influence are the same for both fronts and filaments, despite the mathematical differences explored in *McWilliams and Fox-Kemper* [2013].

The flow configuration used by *McWilliams and Fox-Kemper* [2013] is the following: (1) the flow is uniform along a surface filament; (2) the vertical stratification is stable; (3) from an initial thermal wind configuration that has no Stokes drift (Figure 2a), a Stokes drift that is horizontally uniform, decays vertically, and has $w^S = 0$ arrives impulsively and then is held fixed. The initial state has surface-trapped and along-front jets in thermal wind balance, satisfying

$$\partial_y P + fU = 0, \quad V = 0, \quad W = 0, \quad -\partial_z P + B = 0, \tag{24}$$

where (U, V, W), P, and B are the initial state velocity, pressure, and buoyancy, respectively.

McWilliams and Fox-Kemper [2013] use the WAB equations with no dissipation (a dissipative example is examined in *Suzuki et al.* [2016]). The Stokes drift is horizontally uniform, so the Stokes shear force is purely vertical: $-u_j^L \nabla u_j^S = (0, 0, -\mathbf{u}^L \cdot (\partial_z \mathbf{u}^S))$.

The quantities of interest are the wave-induced deviations from the initial state: namely, $\acute{\mathbf{u}} = \mathbf{u} - \mathbf{U}$, $b' = b - B$, and $p' = p - P$. Their governing equations are obtained by substitution into equation (5) and removal of the initial state balances (24). This results in:
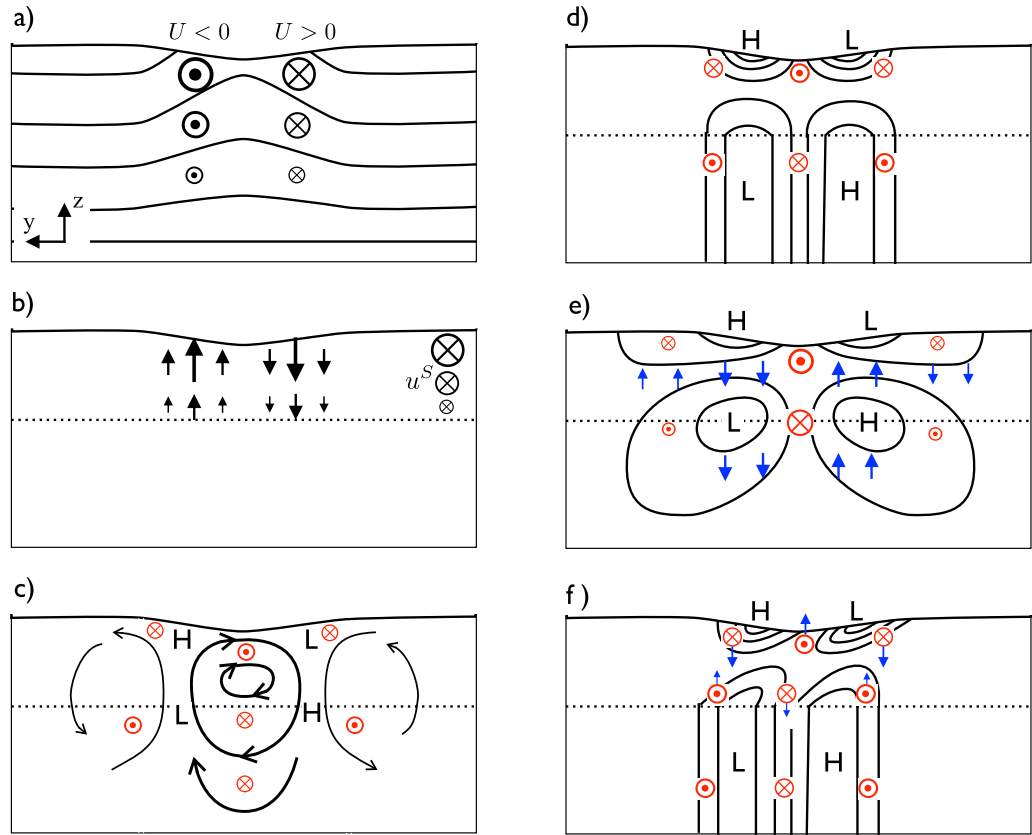
Figure 2. Sketch illustrating the wave influence on a cold filament: (a) the basic state isopycnals and currents; (b) the Stokes shear force (arrows) due to the basic state currents in Figure 2a for a horizontally uniform and positive u^S; (c) the circulation (arrows) and pressure (H and L) patterns driven by the Stokes shear force in Figure 2b; the horizontal velocities of these circulations are turned by the Coriolis force in the directions shown in red until the Coriolis force and the pressure gradient force find a balance; (d) the hydrostatic $\acute{p}$ due to the Stokes shear force in Figure 2b; the horizontal pressure gradient sustains a Lagrangian along-front currents whose directions are shown in red; (e) the hydrostatic $\acute{p}$ due to the sum of the Stokes shear force in Figure 2b and the buoyancy perturbation (blue arrows) produced due to the circulations in Figure 2c; the associated Lagrangian geostrophic currents are shown in red; (f) the hydrostatic $\acute{p}$ due to the sum of the Stokes shear force in Figure 2b and the Stokes shear force (blue arrows) due to the Lagrangian geostrophic currents (red).

$$\partial_t \acute{u} + (\mathbf{u}^L \cdot \nabla)(U + \acute{u}) = -\partial_x \acute{p} + f\acute{v}^L \qquad (25)$$

$$\partial_t \acute{v} + (\mathbf{u}^L \cdot \nabla)\acute{v} \ = -\partial_y \acute{p} - f\acute{u}^L \qquad (26)$$

$$\partial_t \acute{w} + (\mathbf{u}^L \cdot \nabla)\acute{w} \ = -\partial_z \acute{p} + \acute{b} - (U + \acute{u}^L, \acute{v}^L) \cdot (\partial_z u^S, \partial_z v^S) \qquad (27)$$

where $\acute{u}^L = \mathbf{u}^L - \mathbf{U} = \acute{u} + \mathbf{u}^S$. In these equations, $\mathbf{u}^L \cdot \nabla = \acute{v}^L \partial_y + \acute{w}\partial_z$ and $\partial_x \acute{p} = 0$ as V, W, and w^S are all zero, and $\partial_x \phi = 0$ for any quantity ϕ.

First consider the special case where $U = 0$. The arrival of waves induces a horizontally uniform acceleration by the Stokes Coriolis force, $-\mathbf{f} \times \mathbf{u}^S$. The generated Eulerian flow turns due to the Coriolis force on itself ($-\mathbf{f} \times \acute{u}$) until it is directed oppositely to the Stokes drift and $-\mathbf{f} \times \acute{u}$ becomes balanced by part of $-\mathbf{f} \times \mathbf{u}^S$. After inertial oscillations are damped away, the resultant wave-induced deviations in the final steady state are the anti-Stokes flow: $\acute{u} = -\mathbf{u}^S$ or equivalently $\acute{u}^L = (0, 0, 0)$ with $\acute{p} = 0$, and $\acute{b} = 0$. Throughout, the Stokes shear force remains horizontally uniform and hence, is cancelled by a horizontally-uniform $-\partial_z \acute{p}$ that develops to counteract the compression.

This adjustment process to a wave-balanced state shares many dynamical similarities to geostrophic adjustment or adjustment to a change in wind stress [e.g., *Vallis*, 2006], and during adjustment inertial-oscillation-like and internal gravity wave motion is expected. These waves are expected to radiate away or dissipate. The solutions and method used by *McWilliams and Fox-Kemper* [2013] are dissipation-free so the damping and radiation of these modes is not explicitly handled, but the approach is able to determine a final

configuration consistent with conservation of buoyancy and potential vorticity from the initial conditions. Similarly, here the details of the waves produced during adjustment and how they die out are not helpful in gaining intuition about the process, but their existence does help explain inconsistencies between the initial and final state in terms of momentum and energy that may be carried away by the waves. It may be that exact anti-Stokes Eulerian flow is not always the final state after adjustment, but improving on this balance requires directly addressing the complexities of transient evolution under damping and reflection or radiation of waves throughout the whole domain.

Now consider a case with $U \neq 0$. For simplicity, let us consider a Stokes drift with $u^S \geq 0$ and $v^S = 0$. In this case, the anti-Stokes flow is no longer a steady state solution. This is because the anti-Stokes flow leaves the Stokes shear force due to the basic state currents (namely, $-U\partial_z u^S$ in equation (27)) unbalanced. Likewise, simply adding the Stokes drift to U is not a solution, because the Stokes shear force and the Stokes Coriolis force are unbalanced. This Stokes shear force is schematically shown in Figure 2b. When it is unbalanced, it accelerates the local water vertically according to Figure 2b. As a result of pressure perturbations set up by these vertical motions, the Stokes shear force results in the circulation pattern shown in Figure 2c. These circulations are subject to the Lagrangian Coriolis force. Thus, as in geostrophic adjustment, the Coriolis effect turns them until the Coriolis force on the along-front Lagrangian currents $\acute{u}^L$ balances the horizontal pressure gradient force, and the circulations in the $y-z$ plane shut down. The temporary circulations rearrange the density, pressure, and potential vorticity of the initial state to a final stable configuration. If the buoyancy deviation and the Stokes shear force on $\acute{u}^L$ are negligible, the hydrostatic $\acute{p}$ is determined solely by the Stokes shear force on the thermal wind jets (via (29) with a suitable boundary condition, Figure 2d).

After the temporary circulations have shut down, the flow is expected to have $\acute{v}^L = 0$ and $\acute{w}^L = 0$. Then equations (25–27) for the resulting steady state reduce to

$$\partial_y \acute{p} = -f \acute{u}^L \tag{28}$$

$$\partial_z \acute{p} = \acute{b} - (U + \acute{u}^L)\partial_z u^S. \tag{29}$$

Equation (28) is the Lagrangian geostrophic balance. Equation (29) is the wave-influenced quasi-hydrostatic balance, or "wavy hydrostatic" balance of three forces: (1) buoyancy anomaly, (2) the vertical pressure gradient force, and (3) the Stokes shear force on the Lagrangian (initial plus anomalous) currents. Solutions to these equations which are consistent with the initial conditions of buoyancy and potential vorticity are given in *McWilliams and Fox-Kemper* [2013].

Now let us consider the modification of Figure 2d when the buoyancy and potential vorticity deviation are not negligible but the Stokes shear force is weak (small ϵ). The field of $\acute{b}$ produced during the adjustment by the circulations in Figure 2c is sketched in Figure 2e. Thus, $\acute{b}$ is more or less positive and negative where the water moves down and up in Figure 2c, respectively. Below the Stokes shear, the Stokes shear force ceases, but the buoyancy does not. As a result, the field of the hydrostatic $\acute{p}$ acquires vertical gradients below the Stokes shear layer and becomes shallower. The $\acute{p}$ field also becomes wider to balance $\acute{b}$ outside the filament. This effect results in a larger $|\partial_y \acute{p}|$ inside the filament than outside.

Next, let us consider heuristically the modification of Figure 2d when $\acute{b}$ is negligible but $-\acute{u}^L \partial_z u^S$ is not (large ϵ). Because of the alternating pattern of the positive and negative $\acute{u}^L$ in the upper part of the Stokes shear layer in Figure 2d, combining it with the initial flow in Figure 2a causes the extrema of $U + \acute{u}^L$ to move to the right compared to the extrema of U. At depth, the same effect shifts the extrema of $U + \acute{u}^L$ to the left. Correspondingly, the extrema of the hydrostatic $\acute{p}$ shift as shown in Figure 2f.

A final consideration is whether a cross-filament component of the Stokes drift or an along-front perturbation or instability in the buoyancy or potential vorticity might have behavior that is unexpected when compared to wave-free filaments. Based on extending the arguments here and those in *McWilliams and Fox-Kemper* [2013], the cross-frontal flow is expected to arrive at an anti-Stokes balance, which has no cross-front Lagrangian flow, and therefore no Stokes shear force. Thus, the frontal and filamentary effect is expected to be extremely sensitive to direction of the flow versus the Stokes direction [*Suzuki et al.*, 2016]. *Haney et al.* [2015] examine the effects of Stokes forces, including the Stokes shear force, on instabilities of a front. Interestingly, even when the front is wide enough for the Stokes shear force to be negligible on the

front itself and its stability (small ϵ of mean properties), the Stokes shear force can strongly affect the growth rate and structure of instabilities (large ϵ' of perturbations) as shown in section 5.

5. Wave Influence on the Shear-Flow Turbulence, Reynolds Stress, and Ekman Spiral

In the upper boundary layer of the ocean, turbulence is produced by several types of forces; and each of them has its own energy source to produce TKE. In particular, the most important forces and the associated energy sources are (1) Stokes shear force and wave energy as shown in (18), (2) advection and MKE as shown in (16), and (3) buoyancy and potential energy.

Turbulent flows of these types tend to form their own characteristic flow structures such as vortices. Once produced, a turbulent structure of one type may generate a perturbation that triggers a force of a different type (e.g., an advection generating a buoyancy perturbation). Then, the structure becomes forced by multiple forces and forms a hybrid of different turbulence types. In particular, when a Stokes shear force is triggered by a motion of advection-driven or buoyancy-driven turbulence, it can either suppress or enhance the original turbulent motion. Such modification of turbulence, in turn, affects the Reynolds stresses, Ekman spiral, and mixing of the upper boundary layer. The mechanism of the hybrid formation is rooted in the nature of the Stokes shear force, demonstrated here by considering, as an example, the hybrid of Langmuir turbulence and boundary-layer shear-flow turbulence.

5.1. Shear-Flow Turbulence in the Boundary Layer

First, let us summarize important characteristics of boundary-layer shear-flow turbulence. As already mentioned in sections 2 and 3, Langmuir turbulence is the instability that feeds on wave energy transferred by Stokes shear force, and its production does not require a gradient of the Eulerian mean flow nor an unbalanced buoyancy. On the other hand, shear-flow turbulence in the boundary layer (hereafter, shear-flow turbulence) is a type of turbulence that requires a vertical gradient of the Eulerian mean flow for its production. The production is done by vertical advection of the Eulerian mean flow, which causes conversion between MKE and TKE via the shear production term in (15) and (16). MKE converts to TKE when velocity advection reduces the gradient of the Eulerian mean flow, and opposite conversion (i.e., TKE to MKE) occurs when velocity advection increases the shear in the mean flow. The physical reason for the TKE shear production by velocity advection is the following: In general, a water parcel's velocity is a sum of the mean flow and turbulence: $\mathbf{u} = \langle \mathbf{u} \rangle + \mathbf{u}'$ (section 2). When a water parcel moves without an acceleration within a shear flow, its turbulent velocity $\mathbf{u}'$ changes if it moves to a location having a different $\langle \mathbf{u} \rangle$. Thus, this changes the TKE carried by the parcel, even though the parcel's kinetic energy is unchanged. The average of this TKE change is the TKE shear production in (16).

Shear-flow turbulence tends to form vortices [e.g., *Adrian*, 2007]. These vortices are encompassed in a flow that has a larger spatial scale: such as Ekman spiral or baroclinic jet. They are advected by the larger-scale flow and prone to tilt and align in the direction of the gradient of the that flow [*Van Roekel et al.*, 2012; *Hamlington et al.*, 2014]. Because their motions advect the momentum of the larger-scale flow, they act as the Reynolds shear stresses to the larger-scale flow and contribute to the forward cascade of energy.

5.2. Hybrid Turbulence Dynamics

The essence of hybrid turbulence–which derives energy from both Stokes forces and other forces–may be understood using the most basic configuration of the Stokes drift: horizontally uniform, vertically decaying, and $w^S = 0$. Without loss of generality, we may let the direction of the Stokes drift be the positive *x*-direction. Then, $\mathbf{u}^S(z) = (u^S(z), 0, 0)$ where u^S and $\partial_z u^S$ are positive in the Stokes shear layer and zero below it.

As the Stokes drift is horizontally uniform, the Stokes shear force is purely vertical and also $\mathbf{u}^L = \langle \mathbf{u}^L \rangle + \mathbf{u}'$. Thus, the decomposition of the Stokes shear force into the mean and fluctuating parts becomes $-u_j^L \nabla u_j^S = (0, 0, \langle -u^L \partial_z u^S \rangle) + (0, 0, -u' \partial_z u^S)$. The mean part of the Stokes shear force is horizontally uniform. Thus, for an incompressible fluid, it is always cancelled by the pressure gradient force of the horizontally-uniform and wave-influenced hydrostatic pressure $\int_{z'=z}^{0} \langle u^L \partial_{z'} u^S \rangle dz'$. Hence, it is dynamically unimportant. Moreover, it is energetically unimportant as well since it does not contribute to the mean TKE production shown in (18). That is, the average work done to the turbulence by this force is zero:
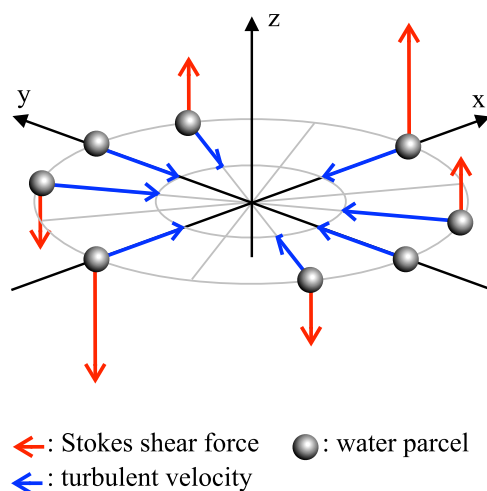
Figure 3. Sketch illustrating the Stokes shear force due to a turbulent velocity. The direction of the Stokes shear $\partial_z \mathbf{u}^S$ is in the positive x-direction.

$\langle \mathbf{u}' \cdot (0,0, \langle -u^L \partial_z u^S \rangle) \rangle = 0$. Thus, only the Stokes shear force anomaly from the horizontal mean contributes to the right hand side of (18): namely, $-\langle u'_i u^L_j \partial_i u^S_j \rangle = \langle \mathbf{u}' \cdot (0,0, -u' \partial_z u^S) \rangle = -\langle w' u' \partial_z u^S \rangle$.

The dynamical role of the Stokes shear force anomaly can be highlighted by subtracting the unimportant balance between the mean Stokes shear force and the associated hydrostatic pressure from (5). Then, (5) becomes

$$\partial_t \mathbf{u} + (\mathbf{u}^L \cdot \nabla)\mathbf{u} = -\nabla \acute{p} - u' \partial_z u^S \hat{\mathbf{z}} + \mathbb{C} \qquad (30)$$

where $\acute{p} = p + \int_{\bar{z}=z}^0 \langle b - u^L \partial_z u^S \rangle d\bar{z}$ is the pressure anomaly from the quasi-hydrostatic pressure; $\hat{\mathbf{z}}$ is the vertical unit vector; and $\mathbb{C} = -\mathbf{f} \times \mathbf{u}^L + b' \hat{\mathbf{z}} + \mathbf{D}^\mathbf{u}$, which vanishes for an inviscid, uniform density fluid without the Coriolis effect.

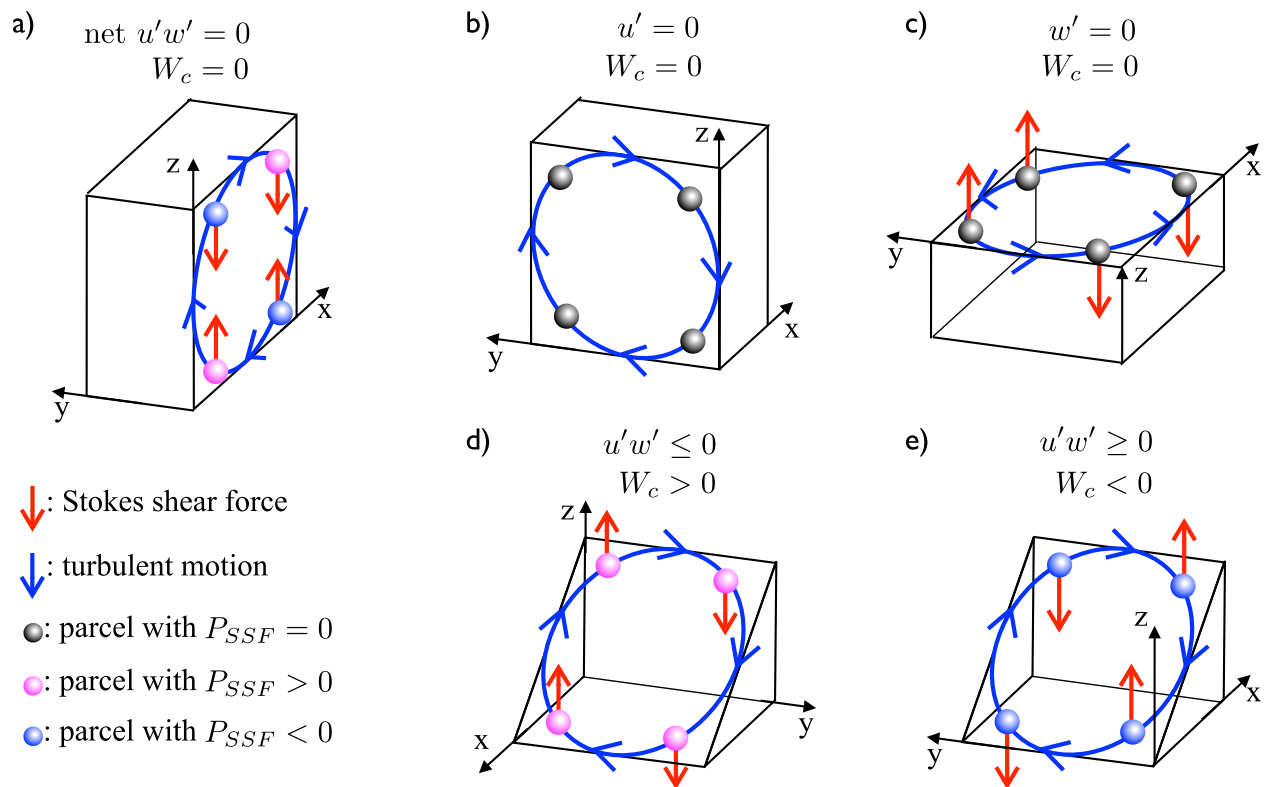Figure 3 and (30) show the nature of the Stokes shear force simply and clearly; the Stokes shear force pushes down a turbulent motion in the direction of the Stokes shear $\partial_z \mathbf{u}^S$ (i.e., a positive u' as $\partial_z u^S$ is positive here) and pushes up a turbulent motion in the opposite direction (here, a negative u'). This force is conditional and directional in the sense that it is triggered only by a turbulent velocity along the Stokes drift direction: that is, u'. Other motions such as v' and w' do not trigger the Stokes shear force.

5.3. Reynolds Stress and the Mean Shear

The Stokes shear force selectively "sorts" u' (turbulent motions along the Stokes shear) by vertical acceleration (Figure 3). This effect produces motions with $u'w' < 0$. The resultant vertical transport of u' by these motions makes the Eulerian mean shear $\partial_z \langle u \rangle$ more negative.

Notice that this sorting is different from "mixing" of fluid, which homogenizes the mean flow and reduces $|\partial_z \langle u \rangle|$. This shear reduction is made by motions with a negative $u'w'$ when $\partial_z \langle u \rangle > 0$ and with a positive $u'w'$ when $\partial_z \langle u \rangle < 0$. This correlation corresponds to a positive TKE shear production in (16); that is, shear-flow turbulence results in mixing, and vice versa. Therefore, the sign of the Reynolds stress $\langle u'w' \rangle$ due to mixing, or shear-flow turbulence, depends on the sign of $\partial_z \langle u \rangle$. This is in contrast with the sorting by Stokes shear force. Stokes shear force produces a negative $u'w'$ regardless of the sign of $\partial_z \langle u \rangle$ because Stokes shear force depends on $\partial_z u^S$ rather than $\partial_z \langle u \rangle$. Therefore, the sorting by Stokes shear force can make a negative mean shear $\partial_z \langle u \rangle$ even more negative.

The velocities along the Stokes drift direction undergo both mixing by shear-flow turbulence and sorting by Stokes shear force. Namely, vertical turbulent advection of the mean flow is a mixing process, but if it produces u', then sorting occurs as well. When $\partial_z \langle u \rangle > 0$, both the mixing and sorting change $\partial_z \langle u \rangle$ toward zero. Both effects make the TKE shear production in the x-direction, $-\langle u'w' \rangle \partial_z \langle u \rangle$, positive as $\partial_z \langle u \rangle > 0$ and $\langle u'w' \rangle < 0$. In contrast, when $\partial_z \langle u \rangle \leq 0$, such as an anti-Stokes flow, then the mixing and sorting compete with one another with mixing reducing and sorting increasing the shear, $|\partial_z \langle u \rangle|$. In this case, the sorting causes transfer of wave energy to the TKE (via the TKE-WE conversion term in equation (18) done by the Stokes shear force) and then from the TKE to the MKE (via the MKE-TKE conversion in equations (15) and (16) done by the vertical advection). If the sorting dominates the mixing, then the TKE shear production in the x-direction, $-\langle u'w' \rangle \partial_z \langle u \rangle$, becomes negative as $\partial_z \langle u \rangle < 0$ and $\langle u'w' \rangle < 0$. Examples of this effect can enhance or weaken modes of energy extraction–or even stabilize or destabilize instabilities–away from their Eulerian shear counterparts [*Haney et al.*, 2015].

While the velocities aligned with the Stokes drift undergo both mixing and sorting, the velocities across the Stokes drift undergo mixing only (Figure 3). Mixing always reduces $|\partial_z \langle v \rangle|$; hence the sign of $\langle v'w' \rangle$ due to mixing is always opposite to the sign of $\partial_z \langle v \rangle$. Stokes shear force affects $\langle v'w' \rangle$ only indirectly via its impact on w' or a correlation between u' and v'.

Figure 4. Sketch illustrating the Stokes shear force exerted on a vortex formed with turbulent motions (u', v', w') and the work done on the vortex by the Stokes shear force. The direction of the Stokes shear $\partial_z \mathbf{u}^S$ is in the positive x-direction. The rotation axis (a) is in the cross-Stokes-drift direction; (b) is in the along-Stokes-drift direction; (c) is in the vertical direction; (d) has a positive slope on the x-z plane; (e) has a negative slope on the x-z plane. P_{SSF} is the work done on the turbulent motion of a water parcel by the Stokes shear force. W_c is the net P_{SSF} along the vortex circulation. If the sense of the circulation is opposite, the blue and red arrows point oppositely. However, the signs of $u'w'$, P_{SSF} (the color of the parcels), and W_c do not change. Notice that Figure 4d has a different camera angle from the other plots.

The mixing of $\langle v \rangle$ and sorting of u' by Stokes shear force is highly anisotropic. As a result, the direction of the Reynolds stress is typically misaligned from the direction of the Eulerian or Lagrangian mean shear. Such a misalignment is evident in numerical simulations [*Van Roekel et al.*, 2012; *McWilliams et al.*, 2012; *Haney et al.*, 2015]. These simulations also reveal a cooccurrence of a highly negative $\langle u'w' \rangle$ with a negative $\partial_z \langle u \rangle$ and a negative shear production due to the sorting, and a large mixing impact on v.

5.4. Enhancement or Suppression of a Hybrid Vortex

From Figure 3, it is clear that the Stokes shear force does positive work on (hence, enhances) a turbulent motion with $u'w' < 0$: namely, a positive (i.e., down-Stokes) u' moving down or a negative (i.e., up-Stokes) u' moving up. On the other hand, it does negative work on (hence, suppresses) a turbulent motion with $u'w' > 0$: namely, a positive u' moving up or a negative u' moving down. More formally, as shown in section 5.2, the TKE production by the Stokes shear force is equal to the work, $P_{SSF} = -w'u'\partial_z u^S$, done on $\mathbf{u}'$ by the Stokes shear force.

Figure 4 schematizes enhancement or suppression of a turbulent vortex structure by the Stokes shear force. When the rotation axis of the vortex is in the cross-Stokes direction (Figure 4a), P_{SSF} and $u'w'$ become locally non-zero. However, the sign of P_{SSF} alternates along the vortex circulation. Hence, the net work W_c done along the circulation diminishes. When the rotation axis is in the along-Stokes or vertical direction (Figures 4b and 4c), P_{SSF} and $u'w'$ are zero everywhere. However, when along-Stokes and vertical vortices are combined, W_c becomes nonzero. More specifically, when a negative vertical rotation and a negative along-Stokes rotation are combined or when a positive vertical rotation and a positive along-Stokes rotation are combined, the axis of the combined rotation has a positive slope on the x-z plane (Figure 4d). In these cases, $u'w' \leq 0$ and $P_{SSF} \geq 0$ everywhere. Therefore, the net work W_c is positive, and the vortex structure gains energy. In contrast, when a negative vertical rotation and a positive along-Stokes rotation are combined or

when a positive vertical rotation and a negative along-Stokes rotation are combined, the combined rotation axis has a negative slope on the x-z plane (Figure 4e). In these cases, the net work W_c is negative, and the vortex structure loses its energy. Note that, when an cross-Stokes vortex and an along-Stokes or vertical vortex are combined, W_c still remains zero.

In a shear flow, only some of the vortices shown in Figure 4 preferentially develop. Figure 5a shows a vortex whose core lies more or less along the Stokes drift in a background mean flow which has a positive $\partial_z \langle u \rangle$. The vortex rotation has an along-Stokes component. On the side of the vortex where the fluid goes up, a water parcel with a slow u from the bottom advects upward and starts to have a negative u'. On the other side, a water parcel with a fast u from the top advects downward and starts to have a positive u'. As a result, the vortex develops a rotation axis tilted as in Figure 4d. Therefore, the vortex circulation gains energy due to the Stokes shear force which appears in the Stokes shear layer.

In contrast, if the background flow has a negative $\partial_z \langle u \rangle$ (Figure 5b), a water parcel starts to have a positive and negative u' as it brings up a slow and down a fast u, respectively. Thus, the rotation axis tilts as in Figure 4e, and the vortex circulation loses its energy due to the Stokes shear force.

In addition to shear-flow turbulence, hybrid modes or altered modes of symmetric instability, geostrophic instability, barotropic instability, etc. occur from Stokes shear forces. *Haney et al.* [2015] detail some of the effects.
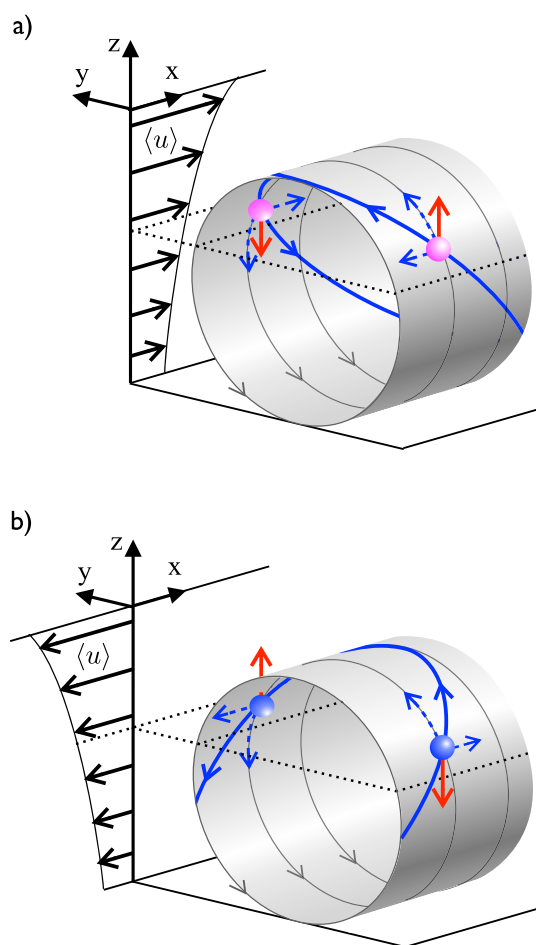

Figure 5. Sketch illustrating the enhancement and suppression of the shear-flow turbulence by the Stokes shear force. In (a), $\partial_z \langle u \rangle > 0$, and in (b), $\partial_z \langle u \rangle < 0$. The location of a vortex core is shown by the gray surface enveloping the core. The depth of the Stokes shear layer is indicated by the doted lines. The colors of the arrows and water parcels are the same as Figure 4. The direction of the Stokes shear $\partial_z \mathbf{u}^S$ is in the positive x-direction.

6. Conclusions

The wave effects in the wave-averaged Boussinesq equations can be formulated in terms of (1) Lagrangian advection, (2) Lagrangian Coriolis force, and (3) Stokes shear force. These forces relate the dynamics and energetics of the WAB equations transparently. Namely, Lagrangian advection transfers energy between the mean flow and turbulence, and the Lagrangian Coriolis force and Stokes shear force transfer energy between waves and the mean flow or turbulence. Lagrangian Coriolis force exists only if the Coriolis effect is nonzero, and Stokes shear force exists only if there is a Stokes drift shear. The form of Stokes shear force clearly distinguishes two types of instabilities that can be produced by Stokes shear force; one is driven by a horizontal gradient of the Stokes drift, and the other is driven by a vertical gradient of the Stokes drift. They often compete with each other by tending to produce flows of opposing circulation. Formulated in this way, each Stokes force scales differently from one another, and also Stokes shear force and buoyancy can be compared easily.

Stokes shear force is the essential force of the CL instabilities [*Craik and Leibovich*, 1976] and the wave-balanced surface fronts [*McWilliams and Fox-Kemper*, 2013; *Suzuki et al.*, 2016]. Stokes shear force acts on motions in the direction of the Stokes shear, which explains both the preference of CL

instabilities to align with the Stokes shear [*Van Roekel et al.*, 2012] and for down-Stokes fronts to be intensified, while up-Stokes fronts are weakened [*Suzuki et al.*, 2016]. The largest component of Stokes shear force is in the vertical direction. Hence, the effect of Stokes shear force on nonhydrostatic or wavy hydrostatic dynamics is again easy to comprehend and could be approximated in a hydrostatic model.

Stokes shear force affects the Reynolds stress and the mean shear of the upper boundary layer by producing Langmuir turbulence or forming hybrids with other types of turbulence. Stokes shear force pushes down a turbulent motion in the direction of the Stokes shear ($\mathbf{u}' \cdot \partial_z \mathbf{u}^S > 0$) and pushes up a turbulent motion in the opposite direction ($\mathbf{u}' \cdot \partial_z \mathbf{u}^S < 0$). Thus, Stokes shear force "sorts" momentum, rather than "mixes" it; that is, if the direction of the Stokes shear $\partial_z \mathbf{u}^S$ is called the positive x-direction, then Stokes shear force makes both $\langle u'w' \rangle$ and $\partial_z \langle u \rangle$ more negative, regardless of the mean shear. As a result, this sorting can make the TKE shear production negative when the Stokes shear opposes the Eulerian shear (a common phenomenon due to anti-Stokes effects). Velocity gradients in the Stokes shear direction undergo both sorting and mixing whereas velocity gradients in the cross-Stokes-shear direction undergo mixing only. This anisotropic effect decorrelates the directions of the mean shear and Reynolds stress.

Although the depth of the Stokes shear layer is typically shallow, Stokes shear force can drive a flow that penetrates well below the Stokes shear layer. Stokes shear force can be triggered by a flow which is being driven by other forces. In such a situation, Stokes shear force can enhance or suppress the original motion. Hybrid dynamics involving Stokes shear force is not limited to shear-flow turbulence. For example, the hybrid dynamics shown in section 5 apply almost directly to the symmetric instability, and the interpretation and scaling of front-wave interactions generalizes to cover mixed-layer eddies and fronts formed by them [*Haney et al.*, 2015; *Suzuki et al.*, 2016]. Horizontal shear instabilities and barotropic instabilities are yet to be studied in detail, but the approach here is applicable to these and many more phenomena.

Appendix A: Converting Between Equation Forms

The conversions between equations (1), (2), (3), and (4) use $\mathbf{u}^L = \mathbf{u} + \mathbf{u}^S$ and a vector identity

$$\alpha \times (\nabla \times \beta) = \alpha_j \nabla \beta_j - (\alpha \cdot \nabla)\beta, \tag{A1}$$

that is true for any vectors $\alpha = (\alpha_1, \alpha_2, \alpha_3)$ and $\beta = (\beta_1, \beta_2, \beta_3)$. Equation (A1) can be shown using a relationship between Levi-Civita symbol and Kronecker delta (sometimes called the "contracted epsilon identity"). Set $\alpha = \mathbf{u}$, $\beta = \mathbf{u}$ for the equivalence between (1) and (2). Likewise, for the conversion between (2) and (3) or (2) and (5), set $\alpha = \mathbf{u}^S$, $\beta = \mathbf{u}$. For the conversion between (2) and (4), use $\alpha = \mathbf{u}$, $\beta = \mathbf{u}^S$ as well as $\alpha = \mathbf{u}^S$, $\beta = \mathbf{u}^L$. A related identity, which is useful for calculating the vorticity equation is

$$\nabla \times [(\alpha \cdot \nabla)\beta] = (\alpha \cdot \nabla)(\nabla \times \beta) + (\nabla \times \beta)(\nabla \cdot \alpha) - [(\nabla \times \beta) \cdot \nabla]\alpha + (\nabla \alpha_j) \times (\nabla \beta_j). \tag{A2}$$

References

Adrian, R. J. (2007), Hairpin vortex organization in wall turbulence, *Phys. Fluids*, *19*, 041301.

Andrews, D. G., and M. E. McIntyre (1978), An exact theory of nonlinear waves on a Lagrangian-mean flow, *J. Fluid Mech.*, *89*, 609–646.

Ardhuin, F., N. Rascle, and K. A. Belibassakis (2008), Explicit wave-averaged primitive equations using a generalized Lagrangian mean, *Ocean Modell.*, *20*(1), 35–60.

Belcher, S. E., et al. (2012), A global perspective on Langmuir turbulence in the ocean surface boundary layer, *Geophys. Res. Lett.*, *39*, L18605, doi:10.1029/2012GL052932.

Bouws, E. (Ed.) (1998), *Guide to Wave Analysis and Forecasting, no*. 702 in WMO, second ed., World Meteorol. Organ., Geneva.

Breivik, Ø., K. Mogensen, J.-R. Bidlot, M. A. Balmaseda, and P. A. Janssen (2015), Surface wave effects in the nemo ocean model: Forced and coupled experiments, *J. Geophys. Res. Oceans*, *120*, 2973–2992, *doi*:10.1002/2014JC010565.

Cavaleri, L., B. Fox-Kemper, and M. Hemer (2012), Wind waves in the coupled climate system, *Bull. Am. Meteorol. Soc.*, *93*(11), 1651–1661.

Chini, G. P., K. Julien, and E. Knobloch (2008), An asymptotically reduced model of Langmuir turbulence, *Geophys. Astrophys. Fluid Dyn.*, *103*(2), 179–197.

Craik, A. D. D., and S. Leibovich (1976), Rational model for Langmuir circulations, *J. Fluid Mech.*, *73*, 401–426.

D'Asaro, E. (2014), Turbulence in the Upper-Ocean Mixed Layer, *Annu. Rev. Mar. Sci.*, *6*(1), 101–115, doi:10.1146/annurev-marine-010213-135138.

D'Asaro, E., J. Thomson, A. Shcherbina, R. Harcourt, M. Cronin, M. Hemer, and B. Fox-Kemper (2014), Quantifying upper ocean turbulence driven by surface waves, *Geophys. Res. Lett.*, *41*, 102–107, doi:10.1002/2013GL058193.

Denbo, D. W., and E. D. Skyllingstad (1996), An ocean large-eddy simulation model with application to deep convection in the Greenland Sea, *J. Geophys. Res.*, *101*(C1), 1095–1110.

Eames, I., and M. E. McIntyre (1999), On the connection between stokes drift and Darwin drift, *Math. Proc. Cambridge Philos. Soc.*, *126*, 171–174.

Fan, Y., and S. M. Griffies (2014), Impacts of parameterized Langmuir turbulence and non-breaking wave mixing in global climate simulations, *J. Clim.*, *27*, 4752–4775.

Garrett, C. (1976), Generation of Langmuir circulations by surface-waves: Feedback mechanism, *J. Mar. Res.*, *34*, 117–130.

Gjaja, I., and D. Holm (1996), Self-consistent Hamiltonian dynamics of wave mean-flow interaction for a rotating stratified incompressible fluid, *Physica D*, *98*(2–4), 343–378.

Hamlington, P. E., L. P. Van Roekel, B. Fox-Kemper, K. Julien, and G. P. Chini (2014), Langmuir-submesoscale interactions: Descriptive analysis of multiscale frontal spin-down simulations, *J. Phys. Oceanogr.*, *44*, 2249–2272.

Haney, S., B. Fox-Kemper, K. Julien, and A. Webb (2015), Symmetric and geostrophic instabilities in the wave-forced ocean mixed layer, *J. Phys. Oceanogr.*, *45*, 3033–3056.

Harcourt, R. R., and E. A. D'Asaro (2008), Large-eddy simulation of Langmuir turbulence in pure wind seas, *J. Phys. Oceanogr.*, *38*(7), 1542–1562, doi:10.1175/2007JPO3842.1.

Hasselmann, K. (1971), On the mass and momentum transfer between short gravity waves and larger-scale motions, *J. Fluid Mech.*, *50*, 189–201.

Holm, D. (1996), The ideal Craik-Leibovich equations, *Physica D*, *98*(2–4), 415–441.

Holthuijsen, L. H. (2007), *Waves in Oceanic and Coastal Waters*, Cambridge Univ. Press, Cambridge.

Huang, C. J., F. Qiao, Z. Song, and T. Ezer (2011), Improving simulations of the upper ocean by inclusion of surface waves in the Mellor-Yamada turbulence scheme, *J. Geophys. Res.*, *116*, C01007, doi:10.1029/2010JC006320.

Komen, G. J., L. Cavaleri, M. Donelan, k Hasselmann, S. Hasselmann, and P. A. E. M. Janssen (1994), *Dynamics and Modelling of Ocean Waves*, Cambridge Univ. Press, Cambridge.

Kukulka, T., A. J. Plueddemann, J. H. Trowbridge, and P. P. Sullivan (2009), Significance of Langmuir circulation in upper ocean mixing: Comparison of observations and simulations, *Geophys. Res. Lett.*, *36*, L10603, doi:10.1029/2009GL037620.

Lane, E. M., J. M. Restrepo, and J. C. McWilliams (2007), Wave-current interaction: A comparison of radiation-stress and vortex-force representations, *J. Phys. Oceanogr.*, *37*(5), 1122–1141, doi:10.1175/JPO3043.1.

Leibovich, S. (1980), On wave-current interaction theories of Langmuir circulations, *J. Fluid Mech.*, *99*, 715–724.

Leibovich, S. (1983), The form and dynamics of Langmuir circulations, *Annu. Rev. Fluid Mech.*, *15*, 391–427.

Lentz, S. J., and M. R. Fewings (2012), The wind and wave-driven inner-shelf circulation, *Annu. Rev. Mar. Sci.*, *4*, 317–343.

Li, K., Z. Zhang, G. Chini, and G. Flierl (2012), Langmuir circulation: An agent for vertical restratification?, *J. Phys. Oceanogr.*, *42*, 1945–1958.

Li, Q., A. Webb, B. Fox-Kemper, A. Craig, G. Danabasoglu, W. G. Large, and M. Vertenstein (2015), Langmuir mixing effects on global climate: WAVEWATCH III in CESM, *Ocean Modell.*, doi:10.1016/j.ocemod.2015.07.020.

Longuet-Higgins, M. S. (1970), Longshore currents generated by obliquely incident sea waves, 1 & 2, *J. Geophys. Res.*, *75*(3), 6778−6801.

Longuet-Higgins, M. S., and R. W. Stewart (1964), Radiation stresses in water waves: A physical discussion, with applications, *Deep Sea Res. Oceanogr. Abstr.*, *11*, 529–562.

Malecha, Z., G. Chini, and K. Julien (2014), A multiscale algorithm for simulating spatially-extended Langmuir circulation dynamics, *J. Comput. Phys.*, *271*, 131–150.

McWilliams, J., and J. Restrepo (1999), The wave-driven ocean circulation, *J. Phys. Oceanogr.*, *29*(10), 2523–2540.

McWilliams, J., J. Restrepo, and E. Lane (2004), An asymptotic theory for the interaction of waves and currents in coastal waters, *J. Fluid Mech.*, *511*, 135–178, doi:10.1017/S0022112004009358.

McWilliams, J. C. (1985), A uniformly valid model spanning the regimes of geostrophic and isotropic, stratified turbulence: Balanced turbulence, *J. Atmos. Sci.*, *42*, 1773–1774.

McWilliams, J. C., and B. Fox-Kemper (2013), Oceanic wave-balanced surface fronts and filaments, *J. Fluid Mech.*, *730*, 464–490, doi:10.1017/jfm.2013.348.

McWilliams, J. C., P. P. Sullivan, and C.-H. Moeng (1997), Langmuir turbulence in the ocean, *J. Fluid Mech.*, *334*, 1–30.

McWilliams, J. C., E. Huckle, J.-H. Liang, and P. P. Sullivan (2012), The wavy Ekman layer: Langmuir circulations, breaking waves, and Reynolds stress, *J. Phys. Oceanogr.*, *42*(11), 1793–1816.

Mei, C. C. (1989), *The Applied Dynamics of Ocean Surface Waves*, vol. 1, World Sci., Singapore.

Mellor, G. (2003), The three-dimensional current and surface wave equations, *J. Phys. Oceanogr.*, *33*(9), 1978–1989.

Monismith, S. G., E. A. Cowen, H. M. Nepf, J. Magnadaudet, and L. Thais (2007), Laboratory observations of mean flows under surface gravity waves, *J. Fluid Mech.*, *573*, 131–147.

Polton, J., D. Lewis, and S. Belcher (2005), The role of wave-induced Coriolis-stokes forcing on the wind-driven mixed layer, *J. Phys. Oceanogr.*, *35*(4), 444–457.

Polton, J. A., and S. E. Belcher (2007), Langmuir turbulence and deeply penetrating jets in an unstratified mixed layer, *J. Geophys. Res.*, *112*, C09020, doi:10.1029/2007JC004205.

Smith, J. A. (2006), Wave-current interactions in finite depth, *J. Phys. Oceanogr.*, *36*, 1403–1419.

Sullivan, P. P., and J. C. McWilliams (2010), Dynamics of winds and currents coupled to surface waves, *Annu. Rev. Fluid Mech.*, *42*, 19–42, doi:10.1146/annurev-fluid-121108-145541.

Sullivan, P. P., J. C. McWilliams, and W. K. Melville (2007), Surface gravity wave effects in the oceanic boundary layer: Large-eddy simulation with vortex force and stochastic breakers, *J. Fluid Mech.*, *593*, 405–452.

Teixeira, M. A. C., and S. E. Belcher (2010), On the structure of Langmuir turbulence, *Ocean Modell.*, *31*(3-4), 105–119, doi:10.1016/j.ocemod.2009.10.007.

Tejada-Martinez, A. E., and C. E. Grosch (2007), Langmuir turbulence in shallow water. Part 2. Large-eddy simulation, *J. Fluid Mech.*, *576*, 63–108.

Thorpe, S. (2004), Langmuir circulation, *Annu. Rev. Fluid Mech.*, *36*, 55–79.

Vallis, G. K. (2006), *Atmospheric and Oceanic Fluid Dynamics: Fundamentals and Large-Scale Circulation*, Cambridge Univ. Press, Cambridge.

Van Roekel, L. P., B. Fox-Kemper, P. P. Sullivan, P. E. Hamlington, and S. R. Haney (2012), The form and orientation of Langmuir cells for misaligned winds and waves, *J. Geophys. Res.*, *117*, C05001, doi:10.1029/2011JC007516.

Webb, A., and B. Fox-Kemper (2011), Wave spectral moments and stokes drift estimation, *Ocean Modell.*, *40*(3-4), 273–288.

Webb, A., and B. Fox-Kemper (2015), Impacts of wave spreading and multidirectional waves on estimating Stokes drift, *Ocean Modell.*, *96*(1), 49–64, doi:10.1016/j.ocemod.2014.12.007.